RSC Advances

ROYAL SOCIETY OF CHEMISTRY

www.rsc.org/advances

Cite this: DOI: 10.1039/c0xx00000x

www.rsc.org/xxxxxx

ARTICLE TYPE

Facile synthesis of Ag nanowires-rGO composites and their promising field emission performance†

Aneeya K Samantara,[1] Dillip Kumar Mishra,[1] Sachin R. Suryawanshi,[2] Mahendra A. More,[2*] Ranjit Thapa,[3] Dattatray J. Late,[4,*] Bikash Kumar Jena,[1,*] Chandra Sekhar Rout[5,*]

Received (in XXX, XXX) Xth XXXXXXXXX 20XX, Accepted Xth XXXXXXXXX 20XX
DOI: 10.1039/b000000x

The crystalline, ultra long silver nanowires (Ag NWs), few layered rGO (reduced graphene oxide) and their rGO-Ag NWs nanocomposite have been synthesized by a polyol reflux technique under optimized experimental conditions. The field emission performance on the rGO-Ag NWs nanocomposite, rGO and AgNWs emitters was investigated. The turn on field required to draw an emission current density of ~1μA/cm^2 was found to be ~5.00, 3.92 and 2.40 V/μm for Ag NWs, rGO and the rGO-Ag NWs nanocomposite emitters, respectively. The combined contribution of the sharp edges of the thin graphene sheets, high aspect ratio of the Ag nanowires, and their synergetic effect in rGO-Ag NWs nanocomposite are responsible for the enhanced field emission behavior The first-principles density functional calculations propose that the enhanced field emission may also be due to the overlapping of the electronic structures of Ag NWs and rGO nanosheets.

1. Introduction

The shape and size of the nanomaterials plays a substantial role in their application in different fields i.e. from electronics to biology. In order to enhance their behavior, the surface architecture is required in which the shape modulation became a dominating factor over their tunable size. For which, so many efforts have been devoted towards development of different shaped nanomaterials with controlled morphology.[1–6] The shape and size controlled nanomaterials of different structures such as one-dimensional (1D) nanorods/nanowires, two-dimensional (2D) nanoplates, three-dimensional (3D) nanocubes and so forth have been explored.[3,4,7–9] Among the other structures, 1D nanowires has been attracted for vast applications in electronics, photovoltaic, biological imaging etc.[10,11] As compared to other metallic nanostructures (Zn, Cu, W, Sn etc.), Ag nanowires (NWs) have been generally applied for the development of sensors, catalysis, memory storage devices and so forth due to their dominating electrical conductivity, thermal stability and structure dependent optical property.[12–16] Recently, networks of AgNWs and graphene hybrid films are observed to present special features and usefulness in optical and electronic devices, catalysis, sensors, etc.[17-19] These hybrid films showed a potential to replace the Indium Tin Oxide (ITO) electrodes due to high optical transparency of 94%, low sheet resistance of 33 Ohm/sq and an excellent stability upon exposure to atmospheric exposure, mechanical pressure and bending.[19]

Some methods have been documented for the synthesis of AgNWs using template based processes.[7,8,20,21] However, these methods limit in the yield for their application. Therefore, the solution phase reactions for high yield synthesis of AgNWs have been followed. Here, we synthesize the Ag NWs by following a solution phase route using $AgNO_3$ as the metal precursor that is reduced to form AgNWs in ethylene glycol medium in the presence of Poly Vinyl Pyrrolidone (PVP). This method, called as the polyol process, has been broadly adopted for the synthesis of different metal nanoparticles.[7,8] On the other hand, the support materials play a vital role to provide stability to nanoparticles and trigger their efficiency for many applications towards catalysis, electro-catalysis, development of different electronic devices and so forth.[22-27] Among the various materials employed as supports, carbon based materials like graphene, carbon nanotubes (single/multi-walled), fullerene, etc. are broadly used. Graphene is a single atom-thick 2D carbon material comprising a honeycomb structure of sp^2 bonded carbon atoms. It has very high electrical conductivity, thermal conductivity, chemical inertness and high surface area to hold the bare nanostructures. Further, the increase in performance of graphene-Ag composite authenticates their development and application. [21] Therefore, facile, single step synthetic approach for the development of such type of composites is still desired.

In this report, we have used a facile single step polyol method for high yield synthesis of reduced graphene-Ag NWs hybrids (rGO-AgNWs). The high electrical conductivity of the Ag/graphene hybrids attracted to investigate its field emission performance for possible applications in the vacuum micro-/nanoelectronic devices. We have investigated field emission properties of the rGO-Ag NWs and compared its performance

with the bare Ag NWs and reduced graphene (rGO) emitters.

2. Experimental Section

2.1 Materials and Synthesis

The Graphite powder, AgCl, $AgNO_3$, KBr, Ethylene glycol were purchased from Sigma-Aldrich. $KMnO_4$, Polyvinyl Pyrrolidone (PVP) were collected from Himedia chemicals. All other chemicals were of analytical grade and used without any further purification. In all the experiments, Millipore water (18Ωm) was used for preparation of the solution.

2.2 Synthesis of Graphene oxide

The graphene oxide (GO) synthesis was carried out by following the modified Hummer's method.[28] In a typical Procedure, 1gm of graphite powder and 25 ml of concentrated H_2SO_4 was taken in a conical flask and stir for 10 minute in an ice bath. Then, 3.5 g of $KMnO_4$ was added slowly and the whole mixture was allowed to stir for two hours in a water bath. On completion of two hours, the conical flask containing aforesaid mixture again placed in the ice bath followed by addition of 50 ml of deionised water. Then sufficient amount of 30% H_2O_2 was added till the effervescence of gas ceases. The obtained brown colored suspension of GO was filtered and repeatedly washed with 0.1M HCl and water for the complete removal of SO_4^{2-} ions. The sample was freeze-dried and stored for future use.

2.3 Synthesis of reduced Graphene oxide (rGO)

20 ml of ethylene glycol was taken in a three-necked round bottom flask and heated to 170^0 C. Once the temperature is maintained then 10 ml of aqueous graphene oxide suspension (1mg/ml) was added drop-wise and leave to stir for next 30 minutes. After that the black colored suspension was collected by centrifugation and washed properly with ethanol.

2.4 Synthesis of Ag NWs

The Ag NW was synthesized by following a single step polyol method.[29] In a typical procedure, a mixture of 0.668 g of Poly Vinyl Pyrrolidone (PVP), 0.01 g of KBr and 20 ml of EG (Ethylene Glycol) taken in a three-necked round bottom flask and heated to maintain a constant temperature of 170 °C. Then, 0.050 g of finely powdered AgCl is added slowly and left the reaction for 3 to 4 minutes. 0.220 g of finely powdered $AgNO_3$ was added slowly to the suspension. The heating was continued for next 30 minutes. After that, the flask containing the solution immediately placed in an ice bath to cool down the solution and stored for prior use.

2.5 Synthesis of rGO-Ag NWs

The synthesis of rGO-Ag NWs composite was carried out by the same synthetic procedure followed for Ag NWs. 10 ml of graphene oxide aqueous solution (1mg/ml) was added drop-wise before placing the round bottom flask in the ice bath and the solution was boiled for another 20 minutes.

2.6 Characterization

The morphology of the as-prepared samples was studied by Scanning electron microscopy (FEG-SEM) measurements at 20 kV acceleration voltage, using a Neon 40 cross-beam system (M/S Carl Zeiss GmbH). The samples for SEM analysis was prepared on the aluminum foil and vacuum dried prior to the analysis. The transmission electron microscopy (TEM) analysis was performed on 200 KeV, JEOL JEM-2010 high resolution transmission electron microscope (HRTEM). The X-ray diffraction patterns were recorded using a Bruker D8 Advance Diffractometer well equipped with a Ni filtered Cu (Kα) radiation of 0.154 nm wavelength (at 40kV, 40mA). The Raman studies of the samples were carried out by Renishaw in Via Raman microscope with an excitation of 514 nm Laser radiation and a 50× objective at 10 second exposure time.

2.7 Field emission

The field emission (FE) current density (*J*) *versus* applied electric field (*E*) and emission current (*I*) *versus* time (*t*) characteristics were measured in a planar 'diode' configuration at the base pressure of ~1.0×10^{-8} mbar. A typical 'diode' configuration consists of a phosphor coated semitransparent screen (a circular disc having diameter ~ 4 cm) as an anode. In order to investigate the FE properties, rGO-Ag NWs composite powder was sprinkled on a piece of carbon tape (radius~2.5 mm). Such rGO-Ag NWs composite sprinkled carbon tape was pasted on a stainless steel holder (diameter ~ 4.5 mm), which acted as a cathode. The FE measurements were carried out at fixed cathode-anode separation of ~ 1 mm. The emission current was measured by Keithely electrometer (6514) by sweeping DC voltage applied to cathode with a step of 40 V (0-40 kV, Spellman, U.S.). The FE current stability was recorded at different preset current values using a computer controlled data acquisition system. Special care has been taken to avoid any leakage current using shielded cables and ensuring proper grounding. Before recording the FE measurements, pre-conditioning of the cathode was carried out by keeping it at ~ 500 volts for 30 min, so as to remove loosely bound particles and/or contaminants by residual gas ion bombardment.

2.8 Computational details

The first principles spin polarized calculations were performed using Vienna Ab initio Simulation Package (VASP) that is based on density functional theory (DFT) calculation using the plane-wave basis set.[30, 31] Core electrons were described with the Projector Augmented Wave (PAW) method.[32] The gradient-corrected functional, developed by Perdew, Burke, and Ernzerhof (PBE), was used to describe the electrons exchange-correlation potentials.[33] The kinetic energy cut-off was set to 400 eV. The k-points meshes were sampled using the scheme of Monkhorst-Pack. All the structures were deemed to have fully relaxed when the total energy converged within 10^{-5} eV/atom and the max force converged within 0.001 eV/ Å.

3. RESULT AND DISCUSSION

3.1 FESEM, XRD, and Raman investigations

Here, we report the synthesis of Ag NWs by a polyol method. In this method, ethylene glycol acts both as a solvent and reducing agent. During the reflux reaction, the silver nitrate gets reduced to form small sized silver nanoparticles followed by the growth of larger particles through Ostwald ripening process. With the assistance of PVP (that controls the growth rate of different faces of silver by means of surface coordination) these larger particles were directed to grow in a definite direction to form nanowires like structures as found in the fig. 1(a).[8] The FESEM images (Fig.1a) show the formation of randomly distributed ultra long nanowires (length up to a few micrometer) having diameter in the range of 55 to 70 nm. It is clearly visible that the Ag NWs have very smooth surface, and some of them are protruding outside the substrate surface Fig. 1 (b) shows the FESEM image the rGO-Ag NWs composite. As it can be seen, the Ag NWs are embedded in the rGO network. A typical XRD pattern of the rGO-Ag NWs nanocomposite (Fig. 2a) exhibits a set of well-defined diffraction peaks which implying its crystalline nature. The observed diffraction peaks could be indexed to the Ag NWs (JCPDS card, No# 04-0783) and rGO phases. Interestingly the XRD pattern does not show diffraction peak(s) corresponding to the other impurity phases, indicating high purity of the as-synthesized product. Thus, the XRD analysis clearly reveals the formation of high purity crystalline rGO-Ag NWs nanocomposite phase under the prevailing experimental conditions.

The as-synthesized GO and rGO has been characterized by different techniques. The folding and the wrinkles present in the GO sheets are clearly visible from the FESEM images (Figure S1a, b, ESI†). The TEM images show the transparency nature of the GO sheets (Figure S1c, ESI†). The existence of well distinguished diffraction points in the SAED pattern (Figure S1d, ESI†), indicates the crystalline nature of GO. This is also supported by the appearance of a sharp XRD peak ($2\theta=10.43^{\circ}$) having interlayer spacing of 0.76 nm (002 plane) (Figure S2, ESI†). But in the case of rGO, this prominent XRD peak pattern disappeared and a small hump was appeared 26° (2θ). This observation revealed the efficient reduction of GO to form rGO. Further, the Raman analysis of the samples were carried out to know the efficient reduction of GO and the formation of the rGO-Ag NWs composites (Figure 2b). In the Raman spectrum of GO and rGO, two prominent peaks appears clearly at 1346 cm^{-1} (D-band), 1585 cm^{-1} (G-band) assigned for the in-plane vibration of k-point phonons of A_{1g} symmetry and first order scattering of the E_{2g} phonon for the in phase stretching vibration of sp^2 carbon atoms, respectively.[25,34] The intensity ratio of D and G band (I_D/I_G) was found to be increased from GO (0.85) to rGO (1.07) standing for the formation of small sized sp^2 domains in the rGO. This observation further confirms the formation of rGO-Ag NWs composite.

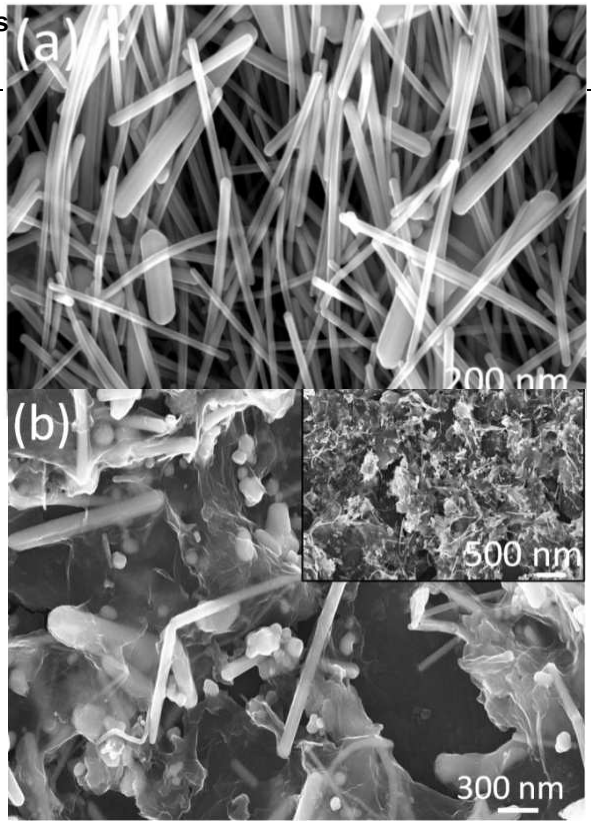

Fig. 1 FESEM images of the Ag NWs (a) and rGO-Ag NW composites (b)

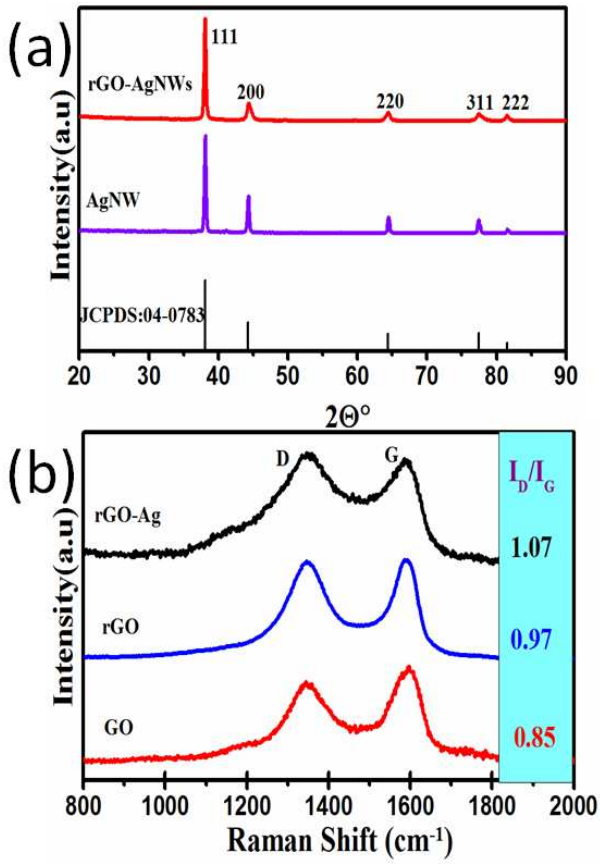

Fig. 2 (a) X-ray diffraction patterns for the as prepared Ag NWs and composite of rGO-Ag NWs. The presence of sharp peaks at $2\theta^{\circ}= 38.11^{\circ}$, 44.38°, 64.38°, 77.37° and 81.48° corresponds to the (111), (200), (220) (311) and (222) planes respectively indexing the face centered cubic (fcc) structure (JCPDS: 04-0783) of the silver nanowires. (b) Raman spectrum of GO, rGO and rGO-Ag NWs composites.

3.2 Field Emission

For comparison, herein we report the FE behaviour of the pristine rGO, AgNWs and rGO-AgNWs nanocomposite

emitters. The characteristic field emission current density versus applied field (J-E) plots of the rGO, AgNWs and rGO-AgNWs nanocomposite emitters are depicted in Fig. 3(a). The values of the turn-on and threshold field, defined as field required to draw an emission current density of ~1μA/cm^2 and ~10μA/cm^2, respectively compiled in Table 1. Furthermore, very high emission current density of ~2.9 mA/cm^2 has been drawn from the rGO-Ag NWs nanocomposite emitter at relatively lower applied field of ~6.80 V/μm (Comparison of field emission parameter of rGO, Ag NWs, rGO-Ag NWs and various reported metal/metal oxide-rGO nanocomposite are compiled in Table 1).

The observed lower values of the turn-on and threshold field are attributed to the high aspect ratio of the Ag NWs, sharp edges of the rGO sheets in the rGO-Ag NWs nanocomposite, owing to their nanometric dimensions. Furthermore, as seen from the FESEM images of the hybrid nanocomposite (charactraized by presence of a few bare Ag NWs, rGO nanosheets covering the Ag NWs), its FE behavior is due to combine effect of high aspect ratio of Ag NWs and rGO nanosheets, along with synergic effect due to formation of heterostructure resulting in modulation of electronic property. Furthermore it can be said that the hybrid nanocomposite emitter exhibits less field screnning effect, and thus the high field enhancement at the 'protruding' Ag NWs and atomically sharp edges of rGO nanosheets is responsible for lowering of the turn-on and threshold values.

The extraction of very high emission current density (~2.9 mA/cm^2) at relatively lower applied field (~6.80 V/μm) can be attributed to its modulation of electronic properties of the hybrid nanocomposite. For field emission, such unique surface topography of the emitter and enhanced electrical property of the hybrid composite should have enhanced its emission behavior. As per the F-N theory, emission of electrons via tunneling through deform potential barrier is exponentially dependent on the work function (ϕ) of the emitter. The difference between potential energy of an electron between Fermi level (E_f) and vacuum level (E_v) is defined as (ϕ). The vacuum level is the potential energy that approaches a nearly constant value in the energy distributions at the vacuum region. Here (3×2$\sqrt{3}$) supercell of Ag (111) surface (three layers) on (2×3-$\sqrt{4}$) supercell of a graphene layer with minimal lattice mismatch has been considered to estimate the work function of the hetro-structure (Ag (111)/graphene). Side view of the model structure is shown in the Fig. 4 (a). The electrostatic potential as a function of coordinate along c-axis of Ag (111)/graphene surface is depicted in the Fig. 4(b). The estimated work function of the Ag(111)/graphene surface has been estimated to be about 4.25 eV, which is about 0.28 eV lesser than pure graphene surface (ϕ = 4.53 eV). The estimated electrostatic potential is shown in Fig.5.

The modified form of the Fowler-Nordehim (F-N) equation for multi-tip emitters deposited on flat substrates is as follows[31-36],

$$J = \lambda_M a \phi^{-1} E^2 \beta^2 \exp\left(-\frac{b\phi^{\frac{3}{2}}}{\beta E} v_F\right) \qquad (1)$$

where J is the emission current density, E is the applied average electric field, a and b are constants, typically 1.54 × 10^{-10} (AV^{-2}eV) and 6.83 × 10^3(VeV$^{-3/2}$μm^{-1}), respectively, φ is the work function of the emitter material, λ_m is a macroscopic pre-exponential correction factor, υ_F is value of the principal Schottky-Nordheim barrier function (a correction factor), and β is the field enhancement factor

Table 1. Turn-on field values of and various metal/metal oxide-rGO nanocomposite reported in the literature

Composite	Turn-on field	Field enhancement factor (β)	Ref.
SnS_2/rGO	1 μA/cm^2 at 2.65 V/μm	3700	37
WS_2/rGO	1 μA/cm^2 at 2.0 V/μm	2978	38
Ag NWs	1 μA/cm^2 at 3.40 V/μm	427	39
Si-ZnO	10 μA/cm^2 at 7.8 V/μm	-	40
RGO	~3.92 V/μm	1013	Present study
Ag NWs	~5.0 V/μm	1047	Present study
rGO-Ag NWs	~2.40 V/μm	~1985	Present study

The Fowler-Nordheim (F-N) plots, derived from the observed J-E characteristic, are shown in fig.3 (b) for the rGO, Ag NWs and rGO-Ag NWs nanocomposite emitter. The ratio of the local electric field to the applied average electric field is nothing but the field enhancement factor ($E_{local} = \beta E_{average}$). The value of β can be estimated from the slope (m) of the F-N plot and, quantifies the degree of enhancement in an electric field at the emission sites due to their nanometric dimension.[37-54] In the present case, the field enhancement factor is calculated from the slope of the F-N plot (fitted linearly).

$$\beta = \frac{-6.8\times10^3 \phi^{3/2}}{m} \qquad (2)$$

Where β represents the field enhancement factor, m is slope of F-N plot and ϕ is the work function of the emitter rGO (4.53 eV), Ag NWs (4.73 eV) and rGO-Ag NWs (4.25 eV calculated using DFT calculations). Thus, the calculated field enhancement factor (β) is ~1013, 1047, 1986, for rGO, Ag NWs and rGO-Ag NWs respectively. Furthermore, the density functional theory (DFT) calculations show that in addition to the surface protrusions and edge effects, the enhanced field emission may also be aptly attributed to the overlapping electronic structure of the composite.

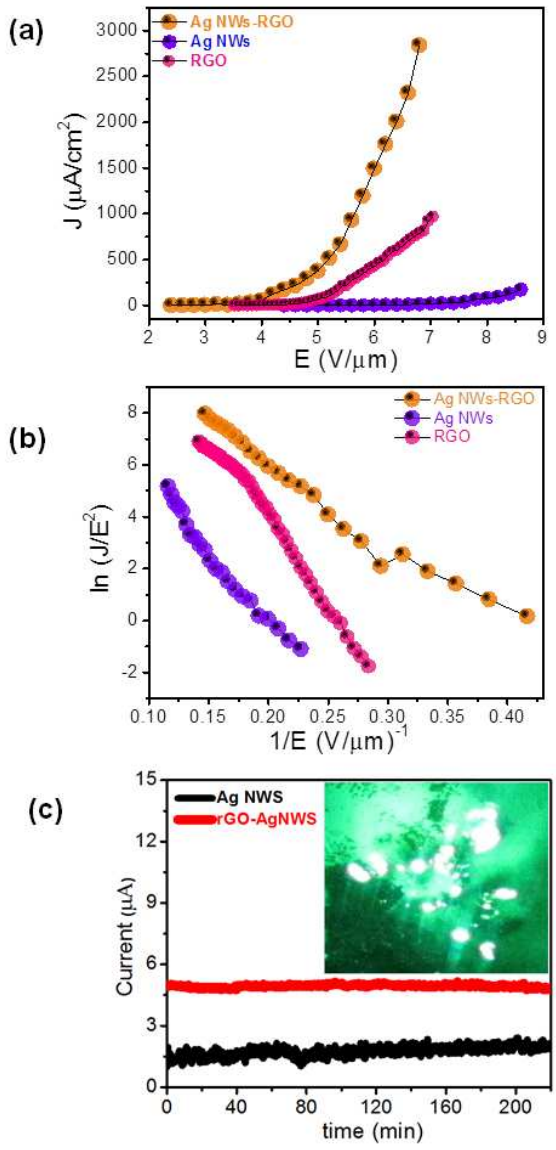

Fig. 3 Field emission characteristics of the rGO, Ag NWs and rGO-Ag NWs nanocomposite emitter **(a)** emission current density versus applied electric field (J-E) curve, **(b)** Fowler-Nordheim (F-N) plot, **(c)** emission current versus time (I-t) plot. The inset of (c) shows typical field emission micrographs of rGO-Ag NWs recorded at current density of ~150 μA/cm^2.

Along with the emission characteristics, current stability is one of the important parameters in the context of practical applications of cold cathodes. Fig. 3(c) depicts the emission current *versus* time (I-t) plot corresponding to preset values of ~1 μA and ~5 μA for Ag NWs and rGO-Ag NWs, respectively recorded over a period of 3 hours at a base pressure of 1 × 10^{-8} mbar. The emission current exhibits small excursions along with 'spike' type fluctuations superimposed on the base level. The average emission current is seen to remain extremely stable in case of rGO-Ag NWs as compared to Ag NWs emitter, which indicates good physical and chemical stability of the emitter. The inset of Fig. 3c shows a typical field emission micrograph of the hybrid rGO-Ag NWs nanocomposite cathode recorded at a current density of ~150 μA/cm^2.

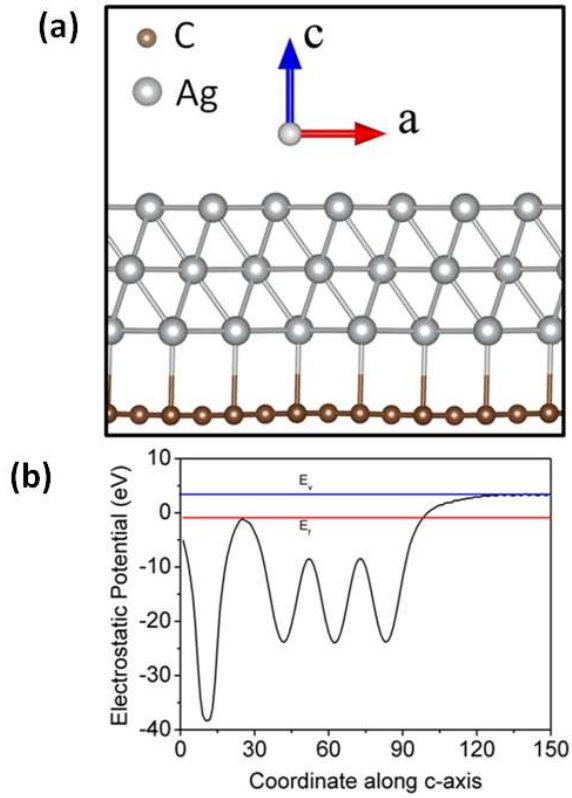

Fig. 4 (a) Side view of Ag (111) on graphene surface, (b) electrostatic potential energy average along x and y axis and plotted along z-axis. E_v and E_f are denoted for vacuum and Fermi energy

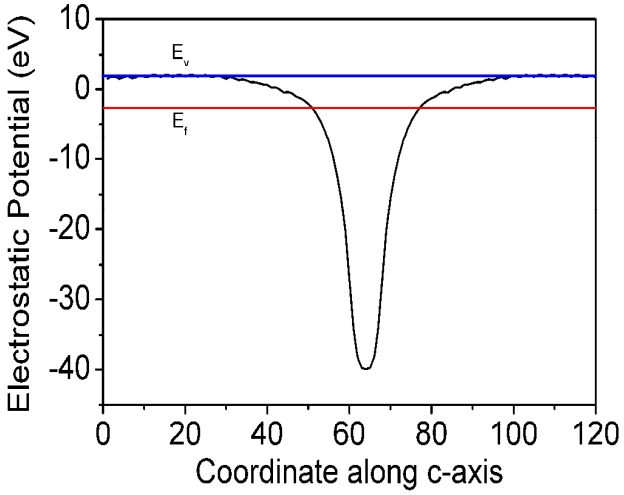

Fig. 5 Electrostatic potential energy of graphene average along x and y axis and plotted along z-axis. E_v and E_f are denoted as vacuum and Fermi energy.

Interestingly, it shows a large number of bright tiny spots, confirming that the emission is indeed from the most protruding Ag NWs and atomically sharp edges of the rGO nanosheets.

The overall superior field emission characteristics suggest that the hybrid rGO-Ag NWs nanocomposite cathode can be considered as a promising electron source for practical applications in various vacuum micro-nano electronic devices.

4. CONCLUSION

In conclusion, Polyol reflux technique was successfully used to synthesize the rGO-Ag NWs composites under optimized experimental condition. Furthermore, the field emission properties of Ag NWs, rGO and rGO-Ag NWs nanocomposite have been investigated at the base pressure of ~$1x10^{-8}$ mbar. The turn on field required to draw a current density of 1μA/cm^2 is found to be 5.0, 3.92 and 2.40 V/μm for Ag NWs, rGO and the rGO-Ag NWs composite, respectively. Enhanced field emission behaviour is observed for rGO-Ag NWs nanocomposite sample due to its high field enhancement factor associated with surface protrusions. In addition, the DFT results show that the enhanced field emission is due to overlapping in electronic structures of Ag NWs and rGO. The outstanding emission current density of rGO-Ag NWs composite at a low turn on field and its nanometric structure morphology can be attracted as a suitable emitter for vacuum micro/nano-electronics and flat panel display device applications.

Acknowledgments

Dr. D. J. Late would like to thank Prof. C. N. R. Rao (FRS) Director ICMS Bangalore (India) and Prof. Vinayak P. Dravid Director NUANCE Centre (Northwestern University) USA for encouragement and support. The research work was supported by Department of Science and Technology (Government of India) for Ramanujan Fellowship to Dr. D. J. Late (Grant No. SR/S2/RJN-130/2012) and Dr. C. S. Rout (Grant No. SR/S2/RJN-21/2012), NCL-MLP project grant 028626, DST-SERB Fast-track Young scientist project Grant No. SB/FT/CS-116/2013, SB/FTP/PS-065/2013 and the partial support by INUP IITB project sponsored by DeitY, MCIT, Government of India and UGC-UKIERI thematic awards (Grant No. UGC-2013-14/005). Aneeya K. Samantara acknowledges CSIR for fellowship. Dr. B. K. Jena acknowledges funding support from MNRE, New Delhi, India (No.102/87/2011-NT), BRNS, Mumbai, India (No.2013/37P/67/BRNS) and CSIR, New Delhi, India (Young Scientist Award Project- YSP-2/2013, P-81-113). Authors are grateful to Prof. B. K. Mishra, Director CSIR-IMMT for his kind permission and encouragement for doing this study. RT thank SRM Research Institute, SRM University for providing supercomputing facility and financial support. Mr. Sachin Suryawanshi gratefully acknowledges the financial support from BARC, Mumbai, for the award of Senior Research Fellowship under BARC-UoP memorandum (Grant No: GOI-E-153). MAM would like to thank the BCUD, Savitribai Phule Pune University, India for the financial support provided for the field emission work under CNQS-UPE-UGC program activity. The Authors thank to Mr. A. Ghosh, IOP, Bhubaneswar for the SEM measurement.

[1]*CSIR-Institute of Minerals and Materials Technology, Bhubaneswar 751013, Odisha, India*
[2]*Department of Physics, Savitribai Phule Pune University Pune-411007, Maharashtra, India*
[3] *SRM Research Institute, SRM University, Kattankulathur, Chennai 603 203, Tamil Nadu, India*
[4]*Physical & Materials Chemistry Division, CSIR-National Chemical Laboratory, Dr. Homi Bhabha Road, Pune 411008. Maharashtra. India*
[5]*School of Basic Sciences, Indian Institute of Technology,* Bhubaneswar *751013, Odisha, India*
datta099@gmail.com/dj.late@ncl.res.in (D.J. Late), csrout@iitbbs.ac.in (C.S. Rout) mam@physics.unipune.ac.in (MAM), ***bikash@immt.res.in*** *(B. K. Jena).*

† Electronic Supplementary Information (ESI) available: [FESEM, TEM and XRD characterizations of GO and rGO. See DOI: 10.1039/b000000x/

Notes and References

1 Y. Sun, Y. Xia, *Science (New York, N.Y.)* 2002, **298,** 2176–2179.
2 H. Shiigi, Y. Yamamoto, N. Yoshi, H. Nakao, T. Nagaoka, *Chem. Commun.* 2006, 4288–4290.
3 I. Pastoriza-Santos, L. M. Liz-Marzan, *J. Mater. Chem.,* 2008, **18,** 1724–1737.
4 B. R. Martin, D. J. Dermody, B. D. Reiss, M. Fang, L. A. Lyon, M. J. Natan, T. E. Mallouk, *Adv. Mater.*, 1999, **11**, 1021–1025.
5 F. Kim, S. Connor, H. Song, T. Kuykendall, P. Yang, *Angew. Chemie Int. Ed.*, 2004, **43**, 3673–3677.
6 (a) M. Grzelczak, J. Perez-Juste, P. Mulvaney, L. M. Liz-Marzan, *Chem. Soc. Rev.*, 2008, **37**, 1783–1791.
7 Y. Sun, B. Gates, B. Mayers, Y. Xia, *Nano Lett.*, 2002, **2**, 165–168.
8 Y.Sun, Y.Xia, *Adv. Mater.*, 2002, **14**, 833–837.
9 H. Chen, L. Shao, Q. Li, J. Wang, *Chem. Soc. Rev.*, 2013, **42**, 2679–2724.
10 M. A. El-Sayed, *Acc. Chem. Res.*, 2001, ***34***, 257–264.
11 V. M. Cepak, C. R. Martin, *J. Phys. Chem. B*, 1998, **102**, 9985–9990.
12 J. M. Renoirt, M. Debliquy, J. Albert, A. Ianoul, C. Caucheteur, *J. Phys. Chem. C*, 2014, **118**, 11035–11042.
13 R. F. Aroca, P. J. G. Goulet, D. S. D. Santos, R. A. Alvarez-Puebla, O. N. Oliveira, *Anal. Chem.* 2005, **77**, 378–382.
14 Y. Cui, I. Y. Phang, R. S. Hegde, Y. H. Lee, X. Y. Ling, *ACS Photonics*, 2014, **1**, 631–637.
15 J. W. Liu, J. L. Wang, W. R. Huang, L. Yu, X. F. Ren, W. C. Wen, S. H. Yu, *Sci. Rep.*, 2012, **2**, *987*.
16 X. Liu, B. Wu, Q. Zhang, J. N. Yip, G. Yu, Q. Xiong, N. Mathews, T. C. Sum, *ACS Nano*, 2014, **8**, 10101-10.17 X. Zhen, L. Zheng, H. Sun, C. Gao, *Adv. Mater.*, 2013, **25**, 3249–3253.18 R. Chen, S. R. Das, C. Jeong, M. R. Khan, D. B. Janes, M. A. Alam, *Adv. Funct. Mater.*, 2013, **23**, 5150–5158.
19 M. S. Lee, K. Lee, S. Y. Kim, H. Lee, J. Park, K. H. Choi, H. K. Kim, D. G. Kim, D. Y. Lee, S. W. Nam, J. U. Park, *Nano Lett.*, 2013, **13**, 2814–2821.
20 Y. J. Han, J. M. Kim, G. D. Stucky, *Chem. Mater.*, 2000, **12**, 2068–2069.
21 S. T. Hsiao, H. W. Tien, W. H. Liao, Y. S. Wang, S. M. Li, C. C. MMa, Y. H. Yu, W. P. Chuang, *J. Mater. Chem. C*, 2014, **2**, 7284–7291.
22 S. S. Kim, Y. R. Kim, T. D. Chung, B. H. Sohn, *Adv. Funct. Mater.*, 2014, **24**, 2764–2771.
23 Y. Ahn, Y. Jeong, Y. Lee, *ACS Appl. Mater. Inter.*, 2012, **4**, 6410–6414.
24 S. C. Sahu, A. K. Samantara, A. Dash, R. R. Juluri, R. K. Sahu, B. K. Mishra, B. K. Jena, *Nano Res.*, 2013, **6**, 635–643.
25 S. C. Sahu, A. K. Samantara, B. Satpati, S. Bhattacharjee, B. K. Jena, *Nanoscale.*, 2013, **5**, 11265–11274.
26 G. Park, L. Bartolome, K. G. Lee, S. J. Lee, D. H. Kim, T. J. Park, *Nanoscale*, 2012, **4**, 3879–3885.

27 G. Goncalves, P. A. A. P. Marques, C. M. Granadeiro, H. I. S. Nogueira, M. K. Singh, J. Grácio, *Chem. Mater.*, 2009, **21**, 4796–4802.

28 W. S. Hummers, R. E. Offeman, *J. Am. Chem. Soc.*, 1958, **80**, 1339-1339.

29 L. Hu, H. S. Kim, J. Y. Lee, P. Peumans, Y. Cui, *ACS Nano*, 2010, **4**, 2955–2963.

30 G. Kresse, J. J. Furthmüller, *Phys. Rev. B*, 1996, **54**, 11169-11186.

31 G. Kresse, J. Furthmüller, *Comput. Mater. Sci.*, 1996, **6**, 15-50.

32 P. E. Blöchl, *Phys. Rev. B*, 1994, ***50***, 17953-17979.

33 J. P. Perdew, K. Burke, M. Ernzerhof, *Phys. Rev. Lett.*, 1996, **77**, 3865-3868.

34 B. Das, R. Voggu, C. S. Rout, C. N. R. Rao, *Chem. Commun.*, 2008, 5155–5157.

35 G. Fursey, Field emission in vacuum microelectronics (Kluwer Academic/ Plenum publishers, New York 2005.

36 R. H. Fowler, L. Proceedings of the Royal Society of London 1928, **119**, 173–181.

37 C. S. Rout, P. D. Joshi, R. V. Kashid, D. S. Joag, M. A. More, A. J. Simbeck, M. Washington, S. K. Nayak and D. J. Late, Appl. Phy. Lett. 2014, **105**, 043109.

38 C. S. Rout, P. D. Joshi, R. V. Kashid, D. S. Joag, M. A. More, A. J. Simbeck, M. Washington, S. K. Nayak, D. J. Late, *Sci. Rep.*, 2013, **3**, 3282.

39 C. Jiang, S. Liu, X. Chen and S. Yu, CrystEngComm 2014, **16**, 8646-8651.

40 R. R. Devarapalli, D. R. Shinde, F. Barka-Bouaifel, S. G. Yenchalwar; R. Boukherroub, M. A. More, M. V. Shelke, J. Mater. Chem. 2012**, 22**, 22922.

41 C. S. Rout, R. Tiwari, R. V. Kashid, D. S. Joag, M. A. More, A. J. Simbeck, M. Washington, S. K. Nayak, D. J. Late, *Europ J. Inorganic Chem.*, 2014, (31) 5331-5336.

42 R. V. Kashid, D. J. Late, S. S. Chou, Y. Huang, M. De, D. S. Joag, M. A. More, V. P. Dravid, *Small.*, 2013, **9**, 2730-2734.

43. B. A. Kakade, V. K. Pillai, D. J. Late, P. G. Chavan, F. J. Sheini, M. A. More, D. S. Joag, Appl. Phys. Lett. 2010, 97, 073102.

44 D. J. Late, P. Misra, B. N. Singh, L. M. Kukreja, D. S. Joag, M. A. More, *Appl. Phy. A* 2009, **95**, 613-620.

45. S. R. Suryawanshi, P. S. Kolhe, C. S. Rout, D. J. Late, M. A More, *Ultramicroscopy* 2015, **149**, 51-57.

46. D. J. Late; M. A. More; D. S. Joag; P. Misra; B. N. Singh; L. M. Kukreja, *App.Phy.s Lett.* 2006, **89,** 123510.

47. D. J. Late; M. A. More; P. Misra; B. N. Singh; L. M. Kukreja; D. S. Joag, *Ultramicroscopy* 2007, **107,** 825-832.

48. D. J. Late; K. S. Date; M. A. More; P. Misra; B. N. Singh; L. M. Kukreja; C. V. Dharmadhikari; D. S. Joag, *Appl. Surf. Sci.2008,* **254,** 3601-3605.

49. D. S. Joag, D. J. Late, U. D. Lanke, Solid State Comm. 2004, **130**, 305-308.

50. R. B. Sharma, D. J. Late, D. S. Joag, A. Govindaraj, C. N. R. Rao, Chem. Phys. Lett. 2006, **428**, 102-108.

51. R. Khare, D. B. Shinde, S. Bansode, M. A. More, M. Majumder, V. K. Pillai, D. J. Late, Appl. Phys. Lett. 2015, 106, 023111.

52. S. Ratha, R. Khare, M. A. More, R. Thapa, D. J. Late, C. S. Rout, RSC Advances, 2015, **5**, 5372-5378.

53. D. J. Late, P. A. Shaikh, R. Khare, R. V. Kashid, M. Chaudhary, M. A. More, S. B. Ogale, ACS Appl. Mater. Interfaces, 2014, 6, 15881-15888

54. K. K. Naik, R. Khare, D. Chakravarty, M. A. More, R. Thapa, D. J. Late, C. S. Rout, Appl. Phys. Lett. 2014, **105**, 233101.

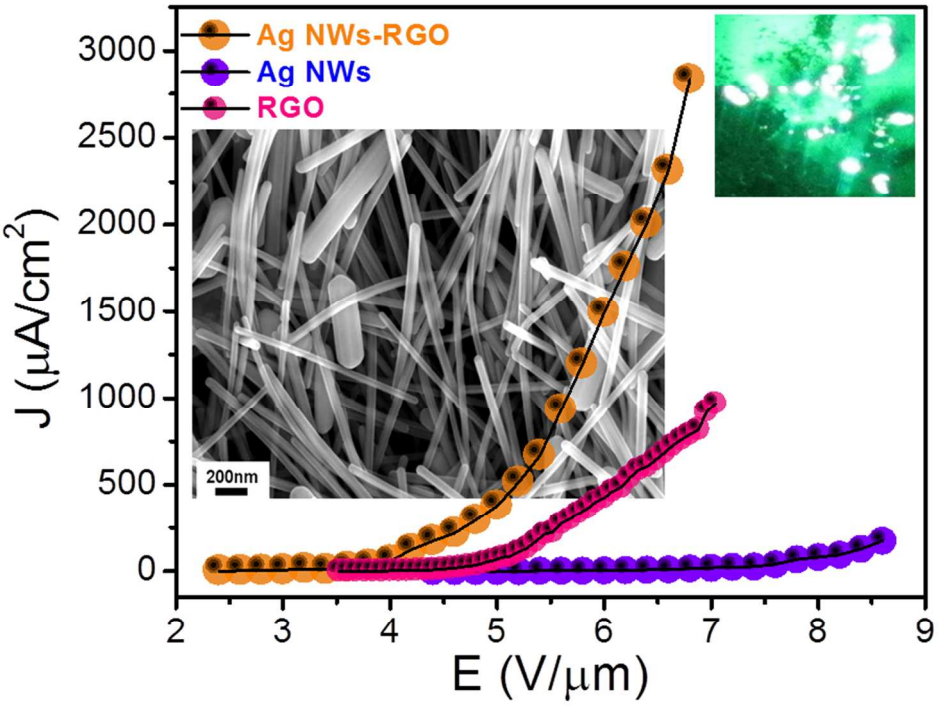

254x190mm (96 x 96 DPI)